

ORIGINAL ARTICLE

Quantitative MRI-Based Analysis Identifies Developmental Limbic Abnormalities in *PCDH19* Encephalopathy

Matteo Lenge^{1,2,3}, Carla Marini⁴, Edoardo Canale⁵, Antonio Napolitano⁶, Salvatore De Masi³, Marina Trivisano⁷, Davide Mei¹, Daniela Longo⁸, Maria Camilla Rossi Espagnet^{8,9}, Ersilia Lucenteforte¹⁰, *PCDH19* Clinical Study Group[†], Carmen Barba¹, Nicola Specchio⁷ and Renzo Guerrini^{1,11}

¹Child Neurology Unit and Laboratories, Neuroscience Department, Children's Hospital A. Meyer – University of Florence, 50139 Florence, Italy, ²Functional and Epilepsy Neurosurgery Unit, Neurosurgery Department, Children's Hospital A. Meyer – University of Florence, 50139 Florence, Italy, ³Clinical Trial Office, Children's Hospital A. Meyer-University of Florence, 50139 Florence, Italy, ⁴Child Neuropsychiatry Unit, Maternal Child Department, University Hospital Ospedali Riuniti, 60100 Ancona, Italy, ⁵Paediatric Neurology and Muscular Diseases Unit, IRCCS 'G. Gaslini' Institute, 16100 Genova, Italy, ⁶Medical Physics Department, Bambino Gesù Children's Hospital, IRCCS, 00100 Rome, Italy, ⁷Rare and Complex Epilepsy Unit, Department of Neuroscience, Bambino Gesù Children's Hospital, IRCCS, 00100 Rome, Italy, ⁸Neuroradiology Unit, Imaging Department, Bambino Gesù Children's Hospital, IRCCS, 00100 Rome, Italy, ⁹NESMOS Department, Sapienza University, 00100 Rome, Italy, ¹⁰Department of Clinical and Experimental Medicine, University of Pisa, 56126 Pisa, Italy and ¹¹IRCCS Stella Maris Foundation, 56018 Pisa, Italy

Address correspondence to Prof. Renzo Guerrini, Neuroscience Department, Children's Hospital A. Meyer – University of Florence, Viale Pieraccini 24, 50139 Firenze, Italy. Email: renzo.guerrini@meyer.it.

[†]See [Appendix](#) for *PCDH19* Clinical Study Group collaborators.

Carmen Barba, Nicola Specchio, and Renzo Guerrini are members of the European Reference Network for rare and complex epilepsies EpiCARE.

Abstract

Protocadherin-19 (*PCDH19*) is a calcium dependent cell-adhesion molecule involved in neuronal circuit formation with prevalent expression in the limbic structures. *PCDH19*-gene mutations cause a developmental encephalopathy with prominent infantile onset focal seizures, variably associated with intellectual disability and autistic features. Diagnostic neuroimaging is usually unrevealing. We used quantitative MRI to investigate the cortex and white matter in a group of 20 *PCDH19*-mutated patients. By a statistical comparison between quantitative features in *PCDH19* brains and in a group of age and sex matched controls, we found that patients exhibited bilateral reductions of local gyrification index (LGI) in limbic cortical areas, including the parahippocampal and entorhinal cortex and the fusiform and lingual gyri, and altered diffusivity features in the underlying white matter. In patients with an earlier onset of seizures, worse psychiatric manifestations and cognitive impairment, reductions of LGI and diffusivity abnormalities in the limbic areas were more pronounced. Developmental abnormalities involving the limbic structures likely represent a measurable anatomic counterpart of the reduced contribution of the *PCDH19* protein to local cortical folding and white matter organization and

are functionally reflected in the phenotypic features involving cognitive and communicative skills as well as local epileptogenesis.

Key words: autism, epilepsy, gyrification index, limbic formation, PCDH19 encephalopathy

Introduction

Mutations of the X-linked *PCDH19* gene (OMIM *300088: EIEE9, epileptic encephalopathy, early infantile, 9) cause a relatively homogeneous phenotype characterized by infantile onset of clusters of focal–febrile–seizures manifesting almost exclusively in females and variably associated with intellectual disability and autistic features (Dibbens et al. 2008; Depienne et al. 2009). Although the clinical context most often corresponds to a developmental and epileptic encephalopathy, about 30% of patients have normal cognitive functions (Trivisano et al. 2018).

About 80% of patients exhibit seizures with prominent affective symptoms that are highly indicative of temporo limbic origin (Marini et al. 2012). In the long term, seizures become less frequent or remit around puberty, cognitive impairment and behavioral disorders reach a plateau and then persist through life (Trivisano et al. 2018).

The *PCDH19* gene related disorder has a unique X-linked female-limited expression wherein causative mutations can be inherited from unaffected fathers; female inheritance is also possible with mildly affected mothers transmitting the mutation to their daughters (Smith et al. 2018). *PCDH19* encodes protocadherin-19 (PCDH19), a calcium dependent cell-adhesion molecule involved in neuronal circuit formation during development and in the maintenance of normal synaptic circuits in adulthood, with regional and temporal expression (Hirano et al. 1999; Kim et al. 2007). *PCDH19* has a prominent expression pattern in the areas connected to the hippocampal formation such as the entorhinal cortex, lateral septum, and basolateral amygdaloid complex (Kim et al. 2010; Pederick et al. 2016, 2018). Studies involving pluripotent stem cells have demonstrated that *PCDH19* plays a role in instructing the apico-basal polarity of the progenitor cells, which is necessary for the proper development of the human brain architecture (Compagnucci et al. 2015). Pederick et al. (2018) demonstrated that *PCDH19* contributes to adhesion specificity in a combinatorial manner such that mosaic expression of *Pcdh19* in heterozygous female mice leads to striking sorting between cell expressing wild-type *PCDH19* and null *PCDH19* in the developing cortex.

Although experimental/animal models highlight the important role played by *PCDH19* in cortical development, MRI studies of patients carrying *PCDH19* mutations report an apparently normal brain morphology in almost all patients; only mild, ill-defined abnormalities of the cortical folding have been observed in some (Kurian et al. 2018; Pederick et al. 2018).

Advanced neuroimaging approaches have the potential to accurately characterize alterations in brain structure associated with neurodevelopmental disorders (Rosas et al. 2002; Sailer et al. 2003; Palaniyappan et al. 2011; Treble et al. 2013; Wallace et al. 2013; Ecker et al. 2015, 2016; Favaro et al. 2015; Duret et al. 2018; Lenge et al. 2018). However, while characterizing morphologic abnormalities and involved networks in clinical subgroups with heterogeneous etiologies remains challenging (Alhusaini et al. 2016), investigating homogeneous subgroups with single gene mutations (Bathelt et al. 2016) or specific copy

number variations (Blackmon et al. 2018) allows more precise correlations.

In this study, we used quantitative neuroimaging models to detect abnormal patterns in brain structures in patients with *PCDH19* mutations.

Methods

Participants

This study includes 20 patients and 40 controls evaluated at two tertiary pediatric neurology centers (A. Meyer Children Hospital, 11 patients and 22 controls; Bambino Gesù Pediatric Hospital, 9 patients and 18 controls). All patients (mean age 14.1 years, median 13.6, range 2.3–26.6) carried a pathogenic *PCDH19* gene mutation (canonical transcript NM_001184880.1) identified by Sanger sequencing, multiplex ligation-dependent probe amplification or next-generation sequencing. Fourteen patients had been included in previous clinical publications (Specchio et al. 2011; Marini et al. 2012; Cappelletti et al. 2015; Trivisano et al. 2018). Controls were matched with patients for acquisition center, sex, and age (± 1 year, mean age 14.2 years, median 13.4, range 3.4–27.0). They were otherwise healthy individuals who had received an MRI for uncomplicated headache. Clinical and genetic data of the 20 patients are described in the following section and summarized in [Supplementary Table 1](#).

Clinical Data

For each patient, clinical and EEG data were collected focusing on age at seizure onset and types of seizures and their provoking factors, ictal and interictal EEG features, neuropsychological profile, behavioral and psychiatric features. Mean age at epilepsy onset was 10.8 months (median 8.0, range 4–28). At onset, 18 patients (90%) exhibited focal seizures, while the remaining two manifested focal to bilateral tonic and tonic-clonic seizures. In 80% of patients, a febrile illness was the triggering factor for seizures, which had occurred in clusters in 95% of them. At follow up, most patients exhibited more than one seizure type, including focal, tonic, tonic-clonic, and absences. In all patients, early development preceding seizure onset was considered to be normal. Eighteen patients developed relevant psychiatric and behavioral disorders, including autism spectrum disorder (ASD, seven patients) or autistic traits (four patients). Six patients had normal cognitive level, while intellectual disability, present in 14, was moderate in six, mild in five, and severe in three.

Genetic Data

All patients carried pathogenic *PCDH19* mutations, 14 (70%) were missense substitutions, 5 (25%) were loss-of-function (2 frameshift, 2 nonsense, and 1 splice-site); one (5%) additional mutation was an in-frame deletion. Two males carried mosaic *PCDH19* mutations (see [Supplementary Table 1](#), Patient 5: 56% mutant population, Patient 14: 90% mutant population). Missense mutations were located throughout the extracellular *PCDH19* region (EC1: 2, EC2: 2, EC2-EC3 linker: 1, EC3: 2, EC4: 4, EC6: 3). Sixteen mutations (80%) occurred de novo. Two patients

had maternally inherited mutations. The study also includes two monozygotic twin pairs, of which one pair carried a de novo mutation, while the other pair had inherited the mutation from an asymptomatic father.

MRI Data Acquisition

Participants underwent MRI acquisitions using the same protocol on both 3 T systems used (Achieva, Philips Healthcare, The Netherlands; Magnetom Skyra, Siemens Healthineers, Germany). MRI assessment of brain structure was performed according to a standard diagnostic protocol for epilepsy (Bernasconi et al. 2019), which included: 3D T1-weighted fast-spoiled gradient echo (3D-T1), 3D T2-weighted fluid attenuation inversion recovery, T2-weighted fast spin-echo, T2*-weighted gradient-eco, and 2D T1-weighted acquisitions. 3D-T1 whole-brain MRIs were acquired by setting both 3 T scanners with the same sequence parameters (acquisition plane sagittal, TR/TE 8.0/3.7 ms, matrix 240 × 240, flip angle 8°, slice thickness 1 mm/no gap, FOV [240 × 240] mm², number of slices 191, voxel resolution [1.0 × 1.0 × 1.0] mm³, acquisition time 6 min, 32 s). Twenty patients and 20 matched controls underwent an additional diffusion-weighted MRI featured by an echo-planar excitation with 40 volumes, including 10 *b*₀ acquisitions and 30 directions covering the whole brain (Philips: TR/TE 4000/80 ms, flip angle 90°, FOV [224 × 224] mm², voxel resolution [2.0 × 2.0 × 2.0] mm³, sense factor 2, acquisition time 4 min, 47 s; Siemens: TR/TE 8100/84 ms, flip angle 90°, FOV [224 × 224] mm², voxel resolution [2.0 × 2.0 × 2.0] mm³, sense factor 2, acquisition time 5 min). The study was approved by the Pediatric Ethics Committee of the Tuscany Region.

MRI Data Analysis

Visual Analysis

Brain MRI images were reviewed searching for structural abnormalities and for artifacts that might hamper computational analyses.

Cortical and Subcortical Gray-Matter Analysis

For a morphometric analysis of cortical and subcortical gray-matter (GM) structures, we processed T1-3D MRI of each subject using FreeSurfer (version 6.0.0, <https://surfer.nmr.mgh.harvard.edu>). The processing pipeline included the following steps: segmentation of subcortical structures (Fischl et al. 2002); cortical segmentation and surface reconstruction of boundaries between white and gray matter (“white” surface) and between GM and cerebrospinal fluid (“pial” surface) (Fischl 2012); parcellation of the cortical surfaces in different gyral and sulcal regions (Fischl et al. 2004). The 3D high-resolution reconstructions of white and pial surfaces were obtained for each hemisphere. Subcortical segmentations and cortical surface reconstructions were visually inspected and manually corrected, where needed. We measured the volume of subcortical structures and the intracranial, subcortical, and cortical volumes of the whole brain.

By adopting a surface-based approach, we assessed the structural properties of the cortex at a whole-brain level. To investigate the process of gyrification, the local gyrification index (LGI), the surface area (SA) and the cortical thickness (CT) were measured for each vertex of the cortical surfaces. LGI quantitatively describes the gyral-sulcal configuration (Zilles et al. 2013) by locally measuring the quantity of infolded cortex (Schaer et al.

2008). CT reflects neural migration/postmigrational organization (Rakic 1988) and GM pruning (Huttenlocher 1990) and is measured by the distance between white and pial surface (Fischl and Dale 2000). SA has been associated to genetics and cognitive abilities (Panizzon et al. 2009) and is calculated as the sum of the areas of the triangles surrounding a vertex.

At a region of interest (ROI) level, we calculated the averaged values of LGI for a subset of regions of the parcellated cortex.

White-Matter Analysis

To investigate potential alterations in the WM, for each subject, we analyzed diffusion MR images by adopting a diffusion tensor imaging (DTI) model. The imaging preprocessing of WM data included the steps for the corrections of motion, eddy currents, and echo-planar imaging-induced distortions (Jenkinson et al. 2012). Diffusion tensor model was fitted to diffusion images (Behrens et al. 2003) to extract diffusivity parameters (fractional anisotropy, FA; mean diffusivity, MD; radial diffusivity, RD; axial diffusivity, AD). Individual diffusion maps were nonlinearly registered to the MNI-ICBM-152 template and projected onto the skeleton generated from the mean FA (cutoff for voxels with FA < 0.2).

At the ROI level, we investigated the integrity of selected WM pathways using the tractography approach of the FSL pipeline (Jenkinson et al. 2012). For each patient, whole-brain tractography was achieved to generate the probability distributions of fiber direction for each voxel, using the “bedpostx” algorithm (number of fibers per voxel 2, burning period 1000, number of jumps 1250, sample every 25). Tract dissection was performed by the “probtrackx” algorithm (radius curvature threshold 0.2, steps per sample 2000, step length 0.5 mm) selecting as seed-masks the clinically relevant or statistically significant areas, including the volumetric projections in the native space of the surface-based LGI ROIs obtained adopting the pipeline proposed by Ecker et al. (2016). In the selected DTI tracts, we calculated the averaged values of the diffusivity parameters and the volume normalized by the local values of the probabilistic distribution (cut-off FA < 0.2).

Statistical Analysis

We carried out statistical analyses on morphometric (cortical GM) and diffusivity (subcortical WM) features using FreeSurfer (Fischl 2012) and FSL (Jenkinson et al. 2012) tools and MATLAB R2019b (Statistics and Machine Learning Toolbox Version 11.6, MathWorks Inc.).

Morphometric Age-Related Statistical Analysis of Cortical Structures

At a whole-brain level, morphometric (LGI, SA, and CT) features were smoothed on the surfaces using a Gaussian kernel (full width at half-maximum [FWHM] = 10 mm). To evaluate the effect of the diagnostic group (Group) and age (Age) on morphometric features (morphGM), we performed a vertex-wise group analysis between PCDH19 patients and controls (CTRLs) by a multivariable linear regression model, using the center (Center) and the age (Age) as covariates and age-by-group variable as interaction term (morphGM = $\beta_0 + \beta_1 \text{Center} + \beta_2 \text{Group} + \beta_3 \text{Age} + \beta_4 [\text{Age} \times \text{Group}]$). Cortical features of each hemisphere were clustered (“mri_surfcluster”) and corrected for multiple comparisons using a Monte-Carlo simulation (“mri_glmfit-sim,” 1000 iterations). For the significant clusters (z-value = 1.3, cluster wise P-value (CWP) < 0.05) of each morphometric feature, we

measured the SA and extracted the location and the z-values of its peaks of maximum values. By the same model, we also assessed the main effect on IGI of the age at MRI and investigated the possible effects of age-by-group interactions (Age \times Group).

Relationship Between Gyrification and Clinical Assessment

For each patient, we selected the clinically relevant cortical ROIs and investigated the effects of averaged IGI on the categorized clinical variables (age at seizure onset, cognitive level and psychiatric disorder [Clinics]) by the following linear regression model: Clinics = $\beta_0 + \beta_1$ Center + β_2 IGI + β_3 Age. Among the selected ROIs we also included the clusters that, at the whole-brain analysis, exhibited a statistically significant between-group difference in IGI.

Volumetric Statistical Analysis of Subcortical Structures

Maintaining the center and age as covariates, we estimated the effect of group on the volumes of subcortical structures using the linear regression model: Volume = $\beta_0 + \beta_1$ Center + β_2 Group + β_3 Age.

White-Matter TBSS Analysis

We obtained the group analysis of WM at a whole-brain level using the tract-based spatial statistics (TBSS) pipeline of FSL software (Smith et al. 2006). Voxel-wise statistical comparison was obtained applying the threshold-free cluster enhancement method (Nichols and Holmes 2002) including the center and the age as covariates (diffWM = $\beta_0 + \beta_1$ Center + β_2 Group + β_3 Age + β_4 [Age \times Group]). The effects on diffusivity parameters (diffWM) of age and age-by-group interaction were also assessed.

Relationship Between Diffusivity Parameters and Clinical Assessment

The selected DTI bundles originating from the IGI-ROIs were tracked by excluding from the algorithm steps cerebellar cortical and brain stem regions, in order to avoid spurious contributions from different diffusivity patterns. Excluded regions were previously segmented in the morphometric analysis and corrected to remove the inaccuracies of automatic segmentation. In the selected DTI tracts, we investigated the effect of diffusivity parameters on categorized clinical variables (age at seizure onset, cognitive level and psychiatric disorder [Clinics]) by adopting a linear regression model (Clinics = $\beta_0 + \beta_1$ Center + β_2 diffWM + β_3 Age) with center and age as covariates.

Results

There were no significant age differences between individuals with PCDH19 and controls ($t = 0.08$, $P = 0.93$).

MRI Visual Analysis

After visual inspection of diagnostic MRI sequences, two patients were excluded from the morphometric (9 and 16) and one from the diffusivity study (16), due to movement artifacts. No malformations of the cortical mantle were observed by visual analysis.

Morphometric Age-Related Analysis of Cortical Structures

The group analysis of cortical measurements revealed morphometric alterations bilaterally involving the mesio-temporal and temporo-occipital regions in the PCDH19 group (Table 1).

Table 1 Whole-brain vertex-wise cluster analysis on IGI, SA, and CT

F-test on IGI	Left hemisphere						Right hemisphere							
	Area	z _{max}	X	Y	Z	CWP	Brain region	Area	z _{max}	X	Y	Z	CWP	Brain region
Main effect of group	3493.90	-3.58	-20.2	-29.4	-13.9	0.002	Para-hippocampal	3350.54	-3.47	27.9	-70.7	-5.5	0.002	Fusiform
Main effect of age	56472.26	-6.51	-33.8	-27.4	51.9	0.002	Postcentral	46385.80	-9.06	47.3	-20.5	44.9	0.002	Postcentral
Age-by-group interaction	None							None						
F-test on SA														
Main effect of group	None							None						
F-test on CT														
Main effect of group	1932.67	2.63	-28.7	-85.6	1.0	0.002	Lateral-occipital	None						

Whole-brain statistical analysis of significant group differences in local gyrification index (IGI), surface area SA, and cortical thickness CT, in left and right hemispheres of patients with PCDH19 mutation and controls (PCDH19 > CTRL, z_{value} = 1.3, cluster wise [CWP] < 0.05), using the center of MRI acquisition and age as covariates. The age-by-group interactions of IGI clusters are represented in the age-related patterns reported in Supplementary Figure 1. Notes: Area, SA of the significant clusters (mm²); X, Y, Z, MNI coordinates of the peak (mm); brain region, region parcellated according to Desikan et al. (2006) labels; none, no significant clusters.

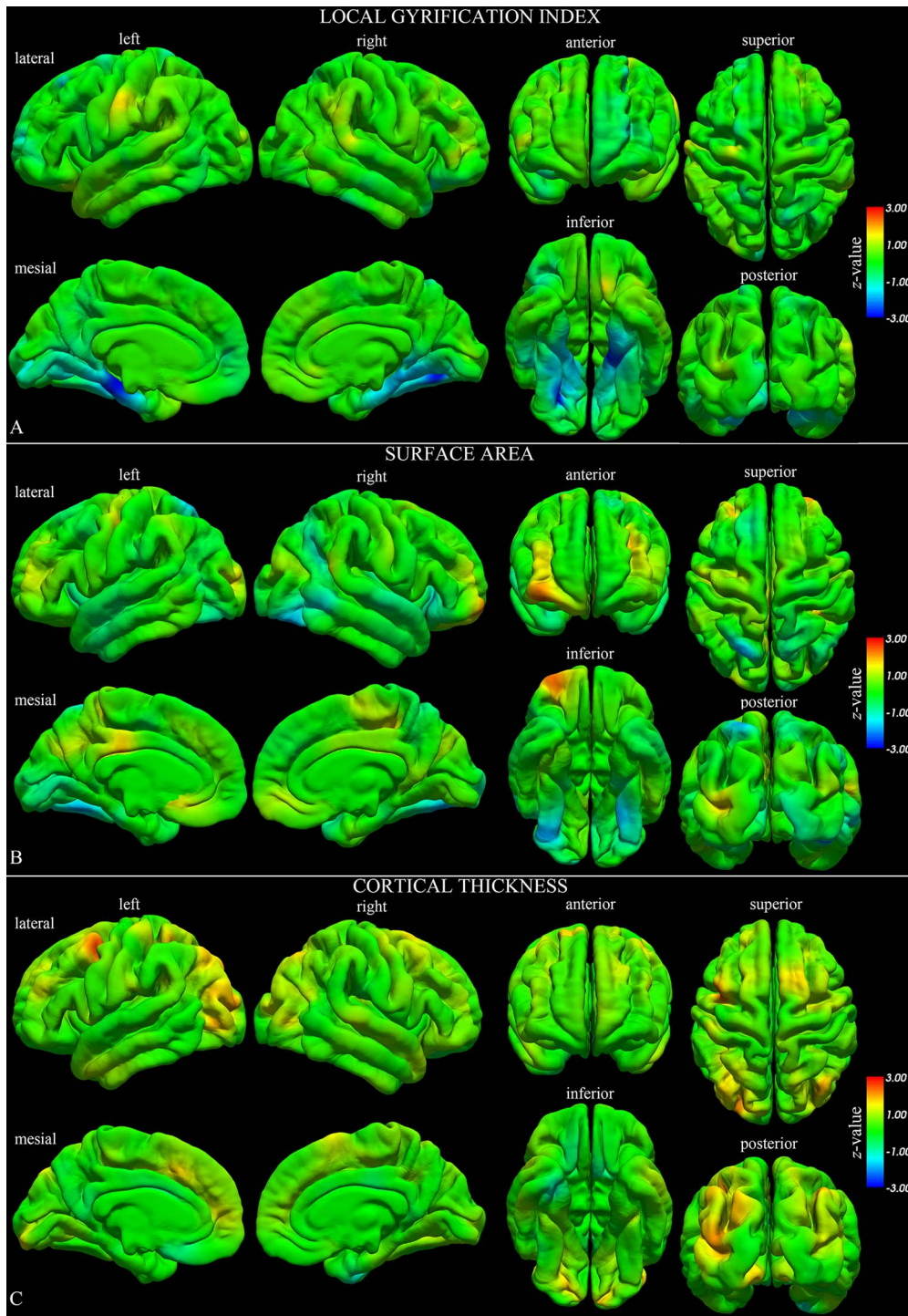


Figure 1. Statistical whole-brain group analysis of PCDH19-related patients compared with matched controls. The results of the statistical analysis on local gyrification index (A), surface area (B), and cortical thickness (C) are represented by z-value maps superimposed on the pial surfaces of left and right hemispheres.

In the gyrification index, we found an effect of group in the limbic cortex of both hemispheres (Table 1 and Fig. 1A). We observed a statistically significant LGI reduction in two bilateral clusters that involved the limbic cortical areas (the parahippocampal, fusiform and lingual gyri and the entorhinal cortex, with values: $z_{\max} = -3.58$, cluster-wise P-value (CWP)=0.002,

area=3493.90 mm², in the left hemisphere; $z_{\max} = -3.47$, CWP=0.002, area=3350.54 mm² in the right hemisphere). The regression analysis revealed no significant effects of the group on SA, although a slightly reduced extension of the cortical mantle was observed in the same areas with significantly reduced LGI (Fig. 1B). The analysis on CT revealed a significant

Table 2 Effect on clinical variables of lGI of selected ROIs in PCDH19

ROI	Side	Clinical variables					
		Age at seizure onset		Cognitive level		Psychiatric disorder	
		β_2	P	β_2	P	β_2	P
lGI cluster	L	30.0461	0.032	-1.9062	0.406	0.3023	0.894
	R	23.8859	0.075	-1.2798	0.555	-1.6653	0.430
Entorhinal	L	23.3909	0.186	0.0662	0.981	-1.4181	0.604
	R	4.9837	0.812	0.4588	0.887	-0.2740	0.931
Parahippocampal	L	30.4976	0.001	-2.1868	0.189	-1.4486	0.380
	R	21.3983	0.030	-4.1076	0.005	-3.4526	0.019
Fusiform	L	27.5233	0.085	1.4675	0.568	1.9369	0.439
	R	23.7327	0.346	1.1387	0.772	-0.3703	0.923
Lingual	L	21.7109	0.072	-1.0894	0.577	1.6209	0.392
	R	5.8399	0.591	1.2334	0.460	0.9955	0.543
Cingulate ^a	L	13.5974	0.289	-1.6428	0.476	-0.2610	0.403
	R	16.6538	0.415	-0.4200	0.574	0.4932	0.474
Medial orbito-frontal	L	14.5592	0.471	-4.1128	0.178	-7.1076	0.010
	R	38.8972	0.068	-2.4358	0.479	-6.2662	0.050
Lateral orbito-frontal	L	24.6992	0.019	-2.3427	0.173	-0.8113	0.638
	R	35.3610	0.004	-2.1992	0.294	-3.4393	0.084
Inferior-temporal	L	9.7361	0.412	1.5465	0.398	1.7411	0.328
	R	3.7691	0.854	3.1797	0.305	4.7066	0.112

Effect on the clinical variables of the PCDH19 group due to the averaged local gyrification index (lGI, [adim]) calculated in the regions (ROIs) of the limbic cortical area (see Fig. 3 for a representative sketch), located in the left (L) and right (R) hemispheres. Data were analyzed by a multivariate linear regression model (Clinics = $\beta_0 + \beta_1$ Center + β_2 lGI + β_3 Age) to explore the effect on the age at seizure onset or the cognitive status or the psychiatric disorder (Clinics, categorical variables in Supplementary Table 1) of the lGI, with the center of acquisition (Center) and age (Age) considered as covariates. β_2 indicates the regression parameters of the model and represents the slope of the regression lines reported in Supplementary Figure 2. Bold indicates significantly altered measures ($P < 0.05$).

^aThe cingulate region includes the isthmus, posterior, caudal anterior, and rostral anterior cingulate regions.

cluster of thicker cortex in the left lateral-occipital gyri (Fig. 1C).

Age-Related Gyrification Patterns

A significant effect of age on gyrification was obtained in two large clusters of reduction centered around the postcentral gyri of both hemispheres; no age-by-group interactions could be found (Table 1). Comparing the age-related cortical patterns obtained in the lGI ROIs of PCDH19-mutated patients with those of controls disclosed a trend of reduction with age exhibiting a similar slope but a significantly lower mean value (see Supplementary Fig. 1).

Relationship Between Gyrification and Clinical Assessment

The effect of lGI on clinical variables (summarized in Supplementary Table 1) was significant for age at seizure onset in several areas of the limbic cortex (Table 2) and revealed that patients with an earlier onset of seizures exhibited lower values of lGI (see Supplementary Fig. 2A). A significant association between cognitive impairment and lGI reduction was observed in the right parahippocampal cortex (see Supplementary Fig. 2B). A status of more severe psychiatric disorder was significantly associated with lower values of lGI in the right parahippocampal cortex and bilaterally in the medial orbito-frontal regions (see Supplementary Fig. 2C).

Volumetric Analysis of Subcortical Structures

The results of volumetric analysis (see Supplementary Table 2) revealed that individuals with PCDH19 mutations had no

significantly altered values in subcortical structures in comparison with controls.

White-Matter TBSS Analysis

TBSS analysis revealed widespread alterations of diffusivity parameters in the white matter of PCDH19-related patients (Table 3 and Fig. 2). The most significant alteration was detected in the corpus callosum (CC), in particular the splenium (sCC) presented a reduction of FA ($t_{\max} = -4.21$, $P = 0.003$) and an increase of RD ($t_{\max} = 5.07$, $P = 0.016$). No statistically significant alterations were detected in MD and AD at the whole-brain level. If age was considered in the model, a significant increase of FA emerged due to myelination processes, with no age-by-group interactions.

Relationship Between Diffusivity Parameters and Clinical Assessment

We selected the corpus callosum (genu [gCC], body [bCC], and [sCC]) and the left and right lGI-ROIs as seeding masks for DTI tracts on which we performed the association analysis between diffusivity and clinical parameters. The DTI tracts originating from the lGI ROIs connected the mesio-temporal limbic cortex to the corpus callosum via the hippocampal cingulum and the fornix bundle (a representative case of a patient is shown in Fig. 3). In the selected DTI fibers, we observed a significant effect of the diffusivity parameters on clinical manifestations, which appeared to be more severe when associated with highly abnormal WM (Table 4). Patients with an earlier onset of seizures exhibited lower FA and higher RD values (see Supplementary Fig. 3A). Worse psychiatric or cognitive conditions tended to be associated

Table 3 Effect of group and age on DTI parameters

Effect of group	No. of voxels	t	P	X	Y	Z	Brain region
FA	48 715	-4.21	0.003	1	-37	9	sCC
MD	None						
RD	46 097	5.07	0.016	3	-38	15	sCC
AD	None						
Effect of age	No. of voxels	t	P	X	Y	Z	Brain region
FA	62 962	16.40	<0.001	5	-22	-19	rCP
MD	None						
RD	None						
AD	None						

TBSS analysis to assess the main effect of group on diffusivity measurements (fractional anisotropy, FA; mean diffusivity, MD; radial diffusivity, RD; axial diffusivity, AD) using the center and the age as covariates. Diffusivity measurements with clusters of significant ($P < 0.05$) alteration are reported. Age-by-group interactions were not observed. No. of voxels, number of voxels of the significant clusters; X, Y, Z, MNI coordinates of the peak (mm); Brain region, region in which the peak is located according to Johns Hopkins University atlas (Hua et al. 2008); sCC, splenium of corpus callosum; rCP, right cerebral peduncle. None, no significant clusters.

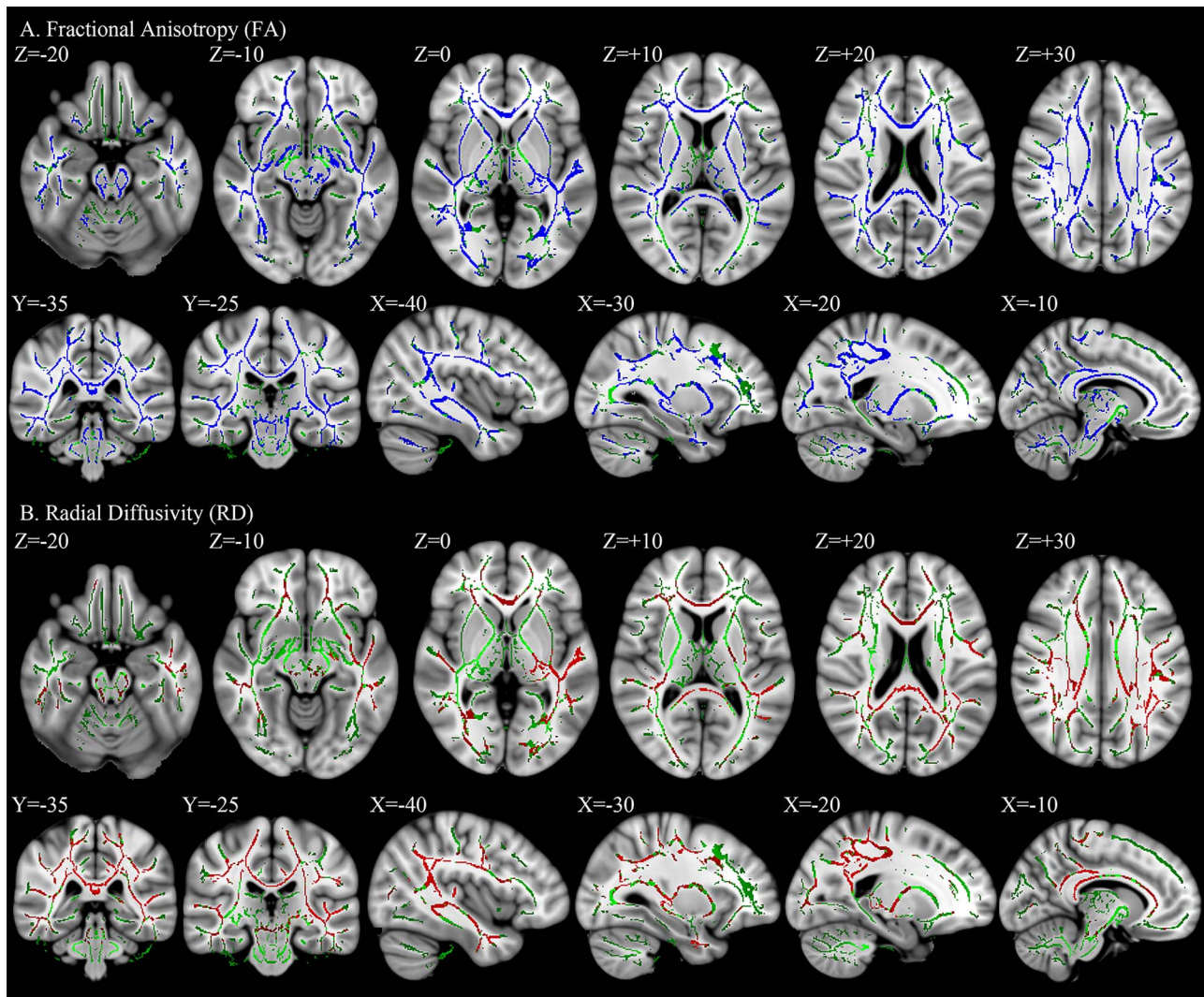


Figure 2. TBSS analysis between PCDH19 and control groups, obtained comparing FA (A) and RD (B) superimposed on the T1-weighted MNI152 brain. Regions of significant ($P < 0.05$) reduction (blue) or increase (red) of diffusion values in the PCDH19 group with respect to controls were superimposed on the mean FA skeleton (green).

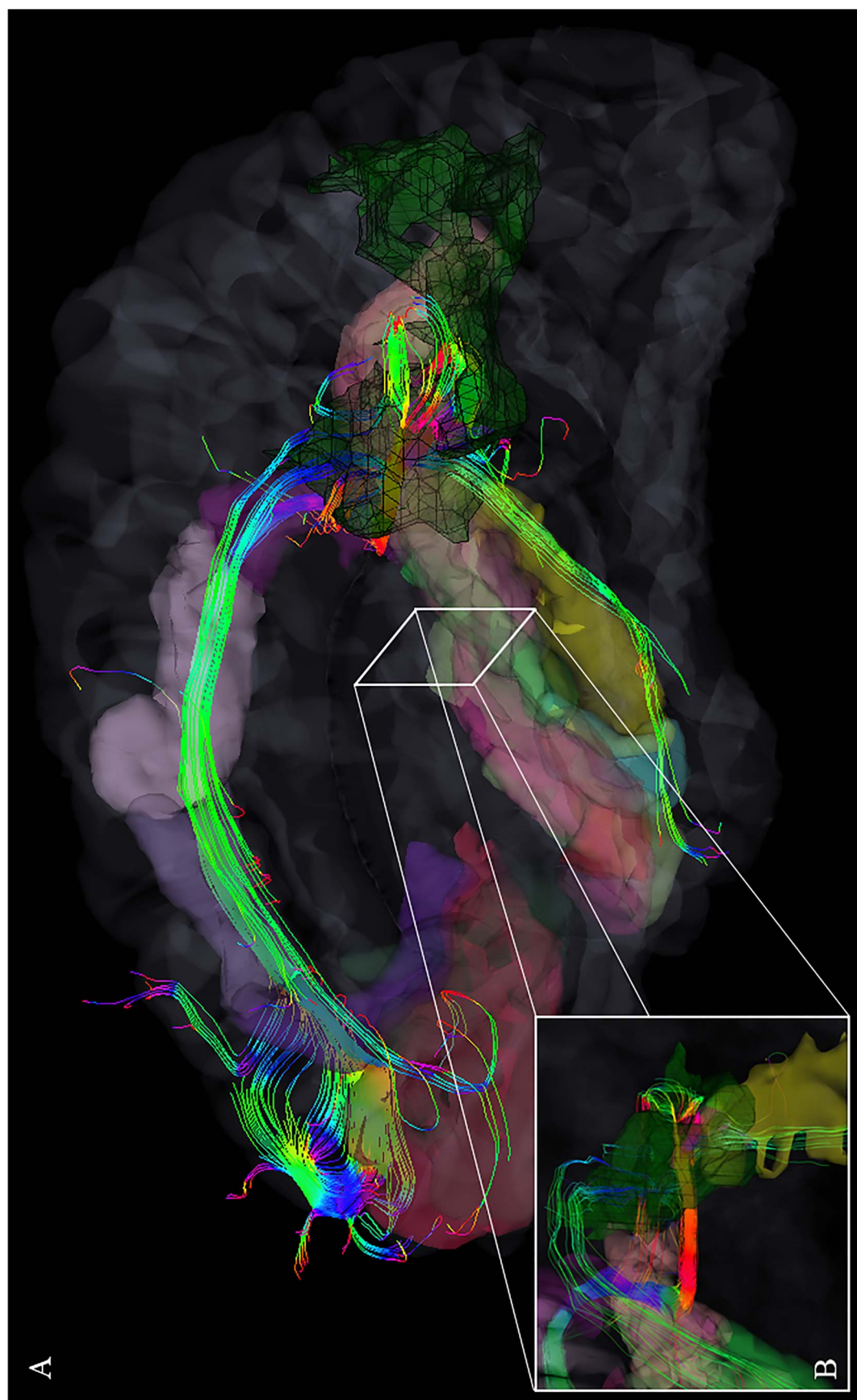


Figure 3. Anatomical structures of the limbic circuit (Bubb et al. 2018) on a patient (no. 7) reconstructed at the different steps of the imaging analysis. DTI tractography of the cingulum bundle (rainbow) is tracked using the IGI-ROI as a seed (green) and branches out toward the inferior portion, that is, the parahippocampal part that runs above the brainstem (gray) and parallel to the hippocampus (yellow) and amygdala (cyan), and the superior portion that overtops the cingulate cortex (purple) up to the orbito-frontal region (magenta). (A) Left lateral view of the 3D model; (B) a planar projection with the structural details of the IGI-ROI and the cingulum branching.

Table 4 Effect on clinical variables of diffusivity parameters of DTI tracts originating from selected ROIs in PCDH19

Diffusivity parameter	ROI-seed	Clinical variable					
		Age at seizure onset		Cognitive level		Psychiatric disorder	
		β_2	P	β_2	P	β_2	P
FA ($\beta_2: \times 10^2$)	Left lGI ROI	0.35	0.001	-0.02	0.278	-0.04	0.050
	Right lGI ROI	0.33	0.005	-0.01	0.588	-0.04	0.084
	sCC	0.72	0.014	-0.11	0.045	-0.11	0.040
	gCC	0.69	0.032	-0.13	0.016	-0.13	0.031
	bCC	0.65	0.046	-0.12	0.031	-0.14	0.020
MD ($\beta_2: \times 10^4$)	Left lGI ROI	-1.05	0.206	-0.07	0.662	0.01	0.935
	Right lGI ROI	-1.52	0.166	-0.10	0.604	0.00	0.993
	sCC	-3.98	0.132	0.41	0.393	0.32	0.525
	gCC	-1.92	0.508	0.12	0.819	0.23	0.672
	bCC	-2.01	0.476	0.25	0.618	0.54	0.293
RD ($\beta_2: \times 10^4$)	Left lGI ROI	-1.33	0.046	-0.01	0.967	0.09	0.502
	Right lGI ROI	-1.66	0.045	-0.04	0.823	0.10	0.524
	sCC	-7.27	0.004	0.88	0.070	0.82	0.106
	gCC	-5.18	0.082	0.73	0.179	0.75	0.179
	bCC	-4.56	0.107	0.75	0.139	1.02	0.046
AD ($\beta_2: \times 10^4$)	Left lGI ROI	0.64	0.457	-0.19	0.206	-0.22	0.158
	Right lGI ROI	0.84	0.449	-0.20	0.323	-0.33	0.098
	sCC	0.33	0.822	-0.10	0.698	-0.15	0.576
	gCC	1.06	0.530	-0.30	0.307	-0.21	0.502
	bCC	0.87	0.616	-0.23	0.446	-0.09	0.778
VOLUME ($\beta_2: \times 10^{-3}$)	Left lGI ROI	9.37	0.062	-0.89	0.340	-0.99	0.304
	Right lGI ROI	-1.79	0.691	0.90	0.250	0.63	0.442
	sCC	0.81	0.170	-0.28	0.002	-0.33	0.001
	gCC	-0.21	0.702	-0.09	0.346	-0.19	0.038
	bCC	0.39	0.285	-0.11	0.087	-0.13	0.040

Effect on the clinical variables (age at seizure onset, cognitive impairment, psychiatric disorder) of diffusivity parameters (fractional anisotropy, FA; mean diffusivity, MD; radial diffusivity, RD; axial diffusivity, AD; volume [mm^3], volume) of the DTI tracts originating from the left and right lGI ROIs and from the splenium (sCC), genu (gCC), and body (bCC) of the corpus callosum. Data were analyzed by a multivariate linear regression model ($\text{Clinics} = \beta_0 + \beta_1 \text{Center} + \beta_2 \text{diffWM} + \beta_3 \text{Age}$) to explore the effect on the clinical variables of PCDH19 patients due to the center of acquisition (Center), diffusivity parameters (diffWM) and age (Age). β_2 indicates the regression parameters of the model and represents the slope of the regression lines reported in [Supplementary Figure 3](#). Bold indicates significantly altered measures ($P < 0.05$).

with more severe patterns of abnormality in WM (FA or volume reduction and RD increase, [Supplementary Fig. 3B, C](#)).

Discussion

We quantitatively examined the imaging features of cortical GM structures in PCDH19-related patients and in controls and found patients to exhibit a bilateral reduction of cortical gyrfication in the mesio-temporal and temporo-occipital regions surrounding limbic structures, associated with normal CT, slightly reduced cortical area and atypical age-related patterns, if compared with controls and cohorts of healthy subjects ([White et al. 2010](#); [Klein et al. 2014](#)).

The gyrfication index describes the patterns of gyri and sulci by which the cortex is structured during brain development ([Schaer et al. 2008](#)). An altered gyrfication indicates a simplified cortical pattern that may be the final effect of an abnormal developmental process at cortical and white-matter level.

Cortical gyrfication is the final result of differential growth mechanisms influenced by genetic, molecular and mechanical determinants ([Llinares-Benadero and Borrell 2019](#)), that start in the fetal epoch and continue throughout life ([Hogstrom et al. 2013](#)). The expansion theories ([Ronan and Fletcher 2014](#); [Ronan et al. 2014](#)) explain gyrfication through mechanisms of differential growths gradients between regions or cortical layers.

Neocortical thickness is proportional to the number of neurons in a column and reflects the developmental processes of migration, postmigrational organization, and maturation ([Huttenlocher 1990](#)), while the SA is related to the number of cortical columns ([Rakic 1988](#)). The genetic contributions to CT and SA are largely distinct ([Chen et al. 2013](#); [Grasby et al. 2020](#)) and the phenotypic and genetic associations between neocortical volume and global cognitive abilities seem to be primarily driven by the cortical SA rather than thickness ([Vuoksima et al. 2015](#)). Indeed, gyrfication helps to increase the SA within a finite space and may improve connectivity by reducing distance between regions ([Docherty et al. 2015](#)). The abnormal cortical pattern we observed in the limbic cortex of patients with PCDH19 mutations may be the ill-effect of irregular growth mechanisms caused by the specific genetic defect and is expected to result functional impairment of the affected cortical areas.

To also investigate the characteristics of the white-matter in the PCDH19-related brain phenotype, we examined between-group differences of diffusivity features and found a widespread reduction of FA combined with increased RD, which was highly significant in the corpus callosum and not associated with volumetric alterations. Abnormalities in the directional diffusions of white-matter bundles, with reduced anisotropy, increased radial, mean and axial diffusivities, may point to a disruption in axonal integrity and delay in myelination and maturation processes ([Drobyshevsky et al. 2007](#)).

Several studies in animal models suggest that PCDH19 influences the migration processes involved in the formation of neural circuits and the maintenance of adult WM connections in the areas connected to the hippocampal formations (Hirano et al. 1999; Kim et al. 2007, 2010; Schaarschuch and Hertel 2018). Pcdh19 functional loss in mutated Zebrafish disrupts the directedness and coherence of cell movements during neurulation (Biswas et al. 2010), impairs columnar organization (Cooper et al. 2015) and determines altered developmental trajectories of network assembly (Light and Jontes 2019). In heterozygous female mice, the mosaic expression of Pcdh19 mutation disrupts cell-adhesion specificity, by a combination of cells expressing wild-type and null PCDH19, and results in abnormal sorting of neuroprogenitor cells in the developing cortex (Pederick et al. 2018).

Experimental animal models highlight the importance of PCDH19 expression patterns for normal development of cortical areas connected to the hippocampal formation (Kim et al. 2010). However, diagnostic structural MRI studies in PCDH19 patients have usually been normal or shown inconsistent abnormalities in cortical folding in a few anecdotal reports (Kurian et al. 2018; Pederick et al. 2018) with an uncertain causal link with the genetic defect. The structural changes we observed in our PCDH19-related cohort are the likely counterpart of subtle developmental abnormalities, resulting in a simplified cortical gyration, associated with altered diffusivity of the underlying white matter.

Local, albeit subtle, malformations in the limbic cortex and in the underlying white matter may correlate with some of the clinical features of the PCDH19-related phenotype. A convincing correlation is feasible with epileptogenesis, which shows in PCDH19 patients a high prevalence of electroclinical seizure patterns with affective symptoms arising from fronto-temporo-occipital limbic regions (Marini et al. 2012; Trivisano et al. 2018), a phenotypic characteristic which is confirmed in the present cohort. Moreover, a statistical correlation was obtained by analyzing the effect of age at seizure onset on the limbic IGI-ROIs, with an earlier onset of seizures, which has been defined the main predictive factor for more severe intellectual disabilities (Kolc et al. 2019), or worsen psychiatric disorders or cognitive impairments (Trivisano et al. 2018), being correlated with a more pronounced gyration and diffusivity abnormalities. Additional features in our PCDH19-related cohort included ASD or autistic traits in 11/20 patients and other behavioral or psychiatric disorders in 7/20. Cognitive and behavioral abnormalities and ASD are among the most frequent and disabling manifestations of PCDH19 encephalopathy (Cappelletti et al. 2015), and may reflect structurally abnormal and dysfunctional limbic structures. A correlation between abnormal mesio-temporal anatomy and autism has previously been reported using MRI in a number of different etiological settings (Travers et al. 2012; Wallace et al. 2013; Ecker et al. 2016; Nickel et al. 2017; Duret et al. 2018). Even though there is wide heterogeneity of identified autism risk genes, many of them converge into similar cellular pathways, including those regulating neurite outgrowth, synapse formation, spine stability and synaptic plasticity (Lin et al. 2016). In our cohort, a significant correlation between autism or cognitive levels and gyration did not emerge, perhaps because only 11 and 7 patients could be included in the analysis, but it might still be proven if larger cohorts were studied.

Although there appear to be convincing anatomo-clinical correlations in our PCDH19 cohort, to the extent that they can be delineated in a complex neurodevelopmental disorder,

some limitations must be pointed out. We included 20 patients with different ages and performed MRI examinations using two different scanners. Patients' enrollment was challenging because PCDH19 encephalopathy is a rare condition, with onset in the pediatric age and associated with impaired cognitive level. For the patients with limited ability to cooperate we were forced to use MR sessions in narcosis. For ethical reasons, we could only enroll patients for whom a brain MRI scan was deemed useful. To reach a sample size large enough to achieve a confident statistical significance, we included in the study patients who had undergone an advanced diagnostic protocol using the two scanners available in two centers. To compensate for the possible effects of center on data analysis, we selected the patients studied by a comparable design protocol for MRI acquisition and adopted a statistical model that compensated possible intercenter biases. The effects of PCDH19 pathology on microstructural WM alterations we observed may be influenced by some factors. DTI measurements are commonly biased by the effect of cross-correlation fibers, particularly in tracts that are narrow and surrounded by tissues with much different diffusion properties (Lee et al. 2009). Better results can be achieved by adopting advanced models that have demonstrated increased resolutions in the analysis of molecular composition and WM microstructure (Fan et al. 2019). We have started a second step analysis with multishell acquisition on a prospectively recruited cohort whose results will be presented in a subsequent report. The structural organization of the limbic regions in PCDH19-related phenotypes may be further investigated by adopting quantitative (Bernhardt et al. 2018) and ultra-high field MRI protocols (De Martino et al. 2018).

Supplementary Material

Supplementary material can be found at *Cerebral Cortex* online.

Funding

This research was supported by the Italian Ministry of Education, University and Research (grant agreement 20172C9HLW).

Conflict of Interest

None declared.

Appendix

The members of the PCDH19 clinical study group who contributed to this research are (in alphabetical order): Annarita Ferrari (IRCCS Stella Maris Foundation, Pisa, Italy), Tiziana Pisano (Neuroscience Department, Children's Hospital A. Meyer-University of Florence, Florence, Italy), Federico Sicca (IRCCS Stella Maris Foundation, Pisa, Italy) and Pasquale Striano (Pediatric Neurology and Muscular Diseases Unit, IRCCS 'G. Gaslini' Institute, Genova, Italy).

References

- Alhusaini S, Whelan CD, Sisodiya SM, Thompson PM. 2016. Quantitative magnetic resonance imaging traits as endophenotypes for genetic mapping in epilepsy. *NeuroImage Clin.* 12:526–534.
- Bathelt J, Astle D, Barnes J, Raymond FL, Baker K. 2016. Structural brain abnormalities in a single gene disorder associated with

- epilepsy, language impairment and intellectual disability. *NeuroImage Clin.* 12:655–665.
- Behrens TEJ, Woolrich MW, Jenkinson M, Johansen-Berg H, Nunes RG, Clare S, Matthews PM, Brady JM, Smith SM. 2003. Characterization and propagation of uncertainty in diffusion-weighted MR imaging. *Magn Reson Med Off J Soc Magn Reson Med/Soc Magn Reson Med.* 50:1077–1088.
- Bernasconi A, Cendes F, Theodore WH, Gill RS, Koepp MJ, Hogan RE, Jackson GD, Federico P, Labate A, Vaudano AE et al. 2019. Recommendations for the use of structural magnetic resonance imaging in the care of patients with epilepsy: a consensus report from the international league against epilepsy neuroimaging task force. *Epilepsia.* 60:1054–1068.
- Bernhardt BC, Fadaie F, Vos de Wael R, Hong SJ, Liu M, Guiot MC, Rudko DA, Bernasconi A, Bernasconi N. 2018. Preferential susceptibility of limbic cortices to microstructural damage in temporal lobe epilepsy: a quantitative T1 mapping study. *Neuroimage.* 182:294–303.
- Biswas S, Emond MR, Jontes JD. 2010. Protocadherin-19 and N-cadherin interact to control cell movements during anterior neurulation. *J Cell Biol.* 191:1029–1041.
- Blackmon K, Thesen T, Green S, Ben-Avi E, Wang X, Fuchs B, Kuzniecky R, Devinsky O. 2018. Focal cortical anomalies and language impairment in 16p11.2 deletion and duplication syndrome. *Cereb Cortex.* 28:2422–2430.
- Bubb EJ, Metzler-Baddeley C, Aggleton JP. 2018. The cingulum bundle: anatomy, function, and dysfunction. *Neurosci Biobehav Rev.* 92:104–127.
- Cappelletti S, Specchio N, Moavero R, Terracciano A, Trivisano M, Pontrelli G, Gentile S, Vigevano F, Cusmai R. 2015. Cognitive development in females with PCDH19 gene-related epilepsy. *Epilepsy Behav.* 42:36–40.
- Chen C-H, Fiecas M, Gutierrez ED, Panizzon MS, Eyler LT, Vuoksimaa E, Thompson WK, Fennema-Notestine C, Hagler DJ, Jernigan TL et al. 2013. Genetic topography of brain morphology. *Proc Natl Acad Sci USA.* 110:17089–17094.
- Compagnucci C, Petrini S, Higurashi N, Trivisano M, Specchio N, Hirose S, Bertini E, Terracciano A. 2015. Characterizing PCDH19 in human induced pluripotent stem cells (iPSCs) and iPSC-derived developing neurons: emerging role of a protein involved in controlling polarity during neurogenesis. *Oncotarget.* 6:26804–26813.
- Cooper SR, Emond MR, Duy PQ, Liebau BG, Wolman MA, Jontes JD. 2015. Protocadherins control the modular assembly of neuronal columns in the zebrafish optic tectum. *J Cell Biol.* 211:807–814.
- De Martino F, Yacoub E, Kemper V, Moerel M, Uludag K, De Weerd P, Ugurbil K, Goebel R, Formisano E. 2018. The impact of ultra-high field MRI on cognitive and computational neuroimaging. *Neuroimage.* 168:366–382.
- Depienne C, Bouteiller D, Keren B, Cheuret E, Poirier K, Trouillard O, Benyahia B, Quelin C, Carpentier W, Julia S et al. 2009. Sporadic infantile epileptic encephalopathy caused by mutations in PCDH19 resembles dravet syndrome but mainly affects females. *PLoS Genet.* 5(2):e1000381.
- Desikan RS, Ségonne F, Fischl B, Quinn BT, Dickerson BC, Blacker D, Buckner RL, Dale AM, Maguire RP, Hyman BT et al. 2006. An automated labeling system for subdividing the human cerebral cortex on MRI scans into gyral based regions of interest. *Neuroimage.* 31:968–980.
- Dibbens LM, Tarpey PS, Hynes K, Bayly MA, Scheffer IE, Smith R, Bomar J, Sutton E, Vandeleur L, Shoubridge C et al. 2008. X-linked protocadherin 19 mutations cause female-limited epilepsy and cognitive impairment. *Nat Genet.* 40:776–781.
- Docherty AR, Hagler DJ, Panizzon MS, Neale MC, Eyler LT, Fennema-Notestine C, Franz CE, Jak A, Lyons MJ, Rinker DA et al. 2015. Does degree of gyrification underlie the phenotypic and genetic associations between cortical surface area and cognitive ability? *Neuroimage.* 106:154–160.
- Drobyshevsky A, Back S, Wyrwicz AM, Li L, Derrick M, Ji X, Kotlajich M, Tan S. 2007. Diffusion tensor imaging of the developing rabbit brain. *Magn Reson Med.* 4:316–329.
- Duret P, Samson F, Pinsard B, Barbeau EB, Boré A, Soulières I, Mottron L. 2018. Gyrification changes are related to cognitive strengths in autism. *NeuroImage Clin.* 20:415–423.
- Ecker C, Andrews D, Dell'Acqua F, Daly E, Murphy C, Catani M, Thiebaut de Schotten M, Baron-Cohen S, Lai MC, Lombardo MV et al. 2016. Relationship between cortical gyrification, white matter connectivity, and autism spectrum disorder. *Cereb Cortex.* 26:3297–3309.
- Ecker C, Bookheimer SY, Murphy DGM. 2015. Neuroimaging in autism spectrum disorder: brain structure and function across the lifespan. *Lancet Neurol.* 4422:1–14.
- Fan Q, Tian Q, Ohringer NA, Nummenmaa A, Witzel T, Tobyne SM, Klawiter EC, Mekkaoui C, Rosen BR, Wald LL et al. 2019. Age-related alterations in axonal microstructure in the corpus callosum measured by high-gradient diffusion MRI. *Neuroimage.* 191:325–336.
- Favaro A, Tenconi E, Degortes D, Manara R, Santonastaso P. 2015. Gyrification brain abnormalities as predictors of outcome in anorexia nervosa. *Hum Brain Mapp.* 36:5113–5122.
- Fischl B. 2012. FreeSurfer. *Neuroimage.* 62:774–781.
- Fischl B, Dale AM. 2000. Measuring the thickness of the human cerebral cortex from magnetic resonance images. *Proc Natl Acad Sci USA.* 97:11050–11055.
- Fischl B, van der KA, Destrieux C, Halgren E, Ségonne F, Salat DH, Busa E, Seidman LJ, Goldstein J, Kennedy D et al. 2004. Automatically parcellating the human cerebral cortex. *Cereb Cortex.* 14:11–22.
- Fischl B, Salat DH, Busa E, Albert M, Dieterich M, Haselgrove C, Van Der Kouwe A, Killiany R, Kennedy D, Klaveness S et al. 2002. Whole brain segmentation: automated labeling of neuroanatomical structures in the human brain. *Neuron.* 33:341–355.
- Grasby KL, Jahanshad N, Painter JN, Colodro-Conde L, Bralten J, Hibar DP, Lind PA, Pizzagalli F, Ching CRK, McMahon MAB et al. 2020. The genetic architecture of the human cerebral cortex. *Science.* 367(6484):aay6690. doi: [10.1126/science.aay6690](https://doi.org/10.1126/science.aay6690).
- Hirano S, Yan Q, Suzuki ST. 1999. Expression of a novel protocadherin, OL-protocadherin, in a subset of functional systems of the developing mouse brain. *J Neurosci.* 19:995–1005. doi: [10.1523/jneurosci.3690-09.2010](https://doi.org/10.1523/jneurosci.3690-09.2010).
- Hogstrom LJ, Westlye LT, Walhovd KB, Fjell AM. 2013. The structure of the cerebral cortex across adult life: age-related patterns of surface area, thickness, and gyrification. *Cereb Cortex.* 23:2521–2530.
- Hua K, Zhang J, Wakana S, Jiang H, Li X, Reich DS, Calabresi PA, Pekar JJ, van Zijl PCM, Mori S. 2008. Tract probability maps in stereotaxic spaces: analyses of white matter anatomy and tract-specific quantification. *Neuroimage.* 39:336–347.
- Huttenlocher PR. 1990. Morphometric study of human cerebral cortex development. *Neuropsychologia.* 28:517–527.
- Jenkinson M, Beckmann CF, Behrens TEJ, Woolrich MW, Smith SM. 2012. Fsl. *Neuroimage.* 62:782–790.

- Kim SY, Chung HS, Sun W, Kim H. 2007. Spatiotemporal expression pattern of non-clustered protocadherin family members in the developing rat brain. *Neuroscience*. 147:996–1021.
- Kim SY, Mo JW, Han S, Choi SY, Han SB, Moon BH, Rhyu IJ, Sun W, Kim H. 2010. The expression of non-clustered protocadherins in adult rat hippocampal formation and the connecting brain regions. *Neuroscience*. 170:189–199.
- Klein D, Rotarska-Jagiela A, Genc E, Sritharan S, Mohr H, Roux F, Han CE, Kaiser M, Singer W, Peter JU. 2014. Adolescent brain maturation and cortical folding: evidence for reductions in gyrification. *PLoS One*. 9(1):e84914.
- Kolc KL, Sadleir LG, Scheffer IE, Ivancevic A, Roberts R, Pham DH, Gecz J. 2019. A systematic review and meta-analysis of 271 PCDH19-variant individuals identifies psychiatric comorbidities, and association of seizure onset and disease severity. *Mol Psychiatry*. 24:241–251.
- Kurian M, Korff CM, Ranza E, Bernasconi A, Lübbig A, Nangia S, Ramelli GP, Wohlrab G, Nordli DR, Bast T. 2018. Focal cortical malformations in children with early infantile epilepsy and PCDH19 mutations: case report. *Dev Med Child Neurol*. 60:100–105.
- Lee JE, Chung MK, Lazar M, DuBray MB, Kim J, Bigler ED, Lainhart JE, Alexander AL. 2009. A study of diffusion tensor imaging by tissue-specific, smoothing-compensated voxel-based analysis. *Neuroimage*. 44:870–883.
- Lenge M, Barba C, Montanaro D, Aghakhanyan G, Frijia F, Guerrini R. 2018. Relationships between morphologic and functional patterns in the polymicrogyric cortex. *Cereb Cortex*. 28:1076–1086.
- Light SEW, Jontes JD. 2019. Multiplane calcium imaging reveals disrupted development of network topology in zebrafish *pcdh19* mutants. *eNeuro*. 6:1–15.
- Lin YC, Frei JA, Kilander MBC, Shen W, Blatt GJ. 2016. A subset of autism-associated genes regulate the structural stability of neurons. *Front Cell Neurosci*. 10:1–35.
- Llinares-Benadero C, Borrell V. 2019. Deconstructing cortical folding: genetic, cellular and mechanical determinants. *Nat Rev Neurosci*. 20:161–176.
- Marini C, Darra F, Specchio N, Mei D, Terracciano A, Parmegiani L, Ferrari A, Sicca F, Mastrangelo M, Spaccini L et al. 2012. Focal seizures with affective symptoms are a major feature of PCDH19 gene-related epilepsy. *Epilepsia*. 53:2111–2119.
- Nichols TE, Holmes AP. 2002. Nonparametric permutation tests for functional neuroimaging: a primer with examples. *Hum Brain Mapp*. 15:1–25.
- Nickel K, Tebartz van Elst L, Perlov E, Endres D, Müller GT, Riedel A, Fangmeier T, Maier S. 2017. Altered white matter integrity in adults with autism spectrum disorder and an IQ >100: a diffusion tensor imaging study. *Acta Psychiatr Scand*. 135:573–583.
- Palaniyappan L, Mallikarjun P, Joseph V, White TP, Liddle PF. 2011. Folding of the prefrontal cortex in schizophrenia: regional differences in gyrification. *Biol Psychiatry, New Insights into the Genetics of Schizophrenia*. 69:974–979.
- Panizzon MS, Fennema-Notestine C, Eyler LT, Jernigan TL, Prom-Wormley E, Neale M, Jacobson K, Lyons MJ, Grant MD, Franz CE et al. 2009. Distinct genetic influences on cortical surface area and cortical thickness. *Cereb Cortex*. 19:2728–2735.
- Pederick DT, Homan CC, Jaehne EJ, Piltz SG, Haines BP, Baune BT, Jolly LA, Hughes JN, Gecz J, Thomas PQ. 2016. *Pcdh19* loss-of-function increases neuronal migration in vitro but is dispensable for brain development in mice. *Sci Rep*. 6:1–10.
- Pederick DT, Richards KL, Piltz SG, Kumar R, Mincheva-Tasheva S, Mandelstam SA, Dale RC, Scheffer IE, Gecz J, Petrou S et al. 2018. Abnormal cell sorting underlies the unique X-linked inheritance of PCDH19 epilepsy. *Neuron*. 97:59–66.e5.
- Rakic P. 1988. Specification of cerebral cortical areas. *Science* (80). 241:170–176.
- Ronan L, Fletcher PC. 2014. From genes to folds: a review of cortical gyrification theory. *Brain Struct Funct*. 220:2475–2483.
- Ronan L, Voets N, Rua C, Alexander-Bloch A, Hough M, Mackay C, Crow TJ, James A, Giedd JN, Fletcher PC. 2014. Differential tangential expansion as a mechanism for cortical gyrification. *Cereb Cortex*. 24:2219–2228.
- Rosas HD, Liu AK, Hersch S, Glessner M, Ferrante RJ, Salat DH, van der Kouwe A, Jenkins BG, Dale AM, Fischl B. 2002. Regional and progressive thinning of the cortical ribbon in Huntington's disease. *Neurology*. 58:695–701.
- Sailer M, Fischl B, Salat D, Tempelmann C, Schönfeld MA, Busa E, Bodammer N, Heinze H-J, Dale A. 2003. Focal thinning of the cerebral cortex in multiple sclerosis. *Brain*. 126:1734–1744.
- Schaarschuch A, Hertel N. 2018. Expression profile of N-cadherin and protocadherin-19 in postnatal mouse limbic structures. *J Comp Neurol*. 526:663–680.
- Schaer M, Cuadra MBB, Tamarit L, Lazeyras F, Eliez S, Thiran J. 2008. A surface-based approach to quantify local cortical gyrification. *IEEE Trans Med Imaging*. 27:161–170.
- Smith L, Singhal N, El Achkar CM, Truglio G, Rosen Sheidley B, Sullivan J, Poduri A. 2018. PCDH19-related epilepsy is associated with a broad neurodevelopmental spectrum. *Epilepsia*. 59:679–689.
- Smith SM, Jenkinson M, Johansen-Berg H. 2006. Tract-based spatial statistics: voxelwise analysis of multi-subject diffusion data. *Neuroimage*. 31:1487–1505.
- Specchio N, Marini C, Terracciano A, Mei D, Trivisano M, Sicca F, Fusco L, Cusmai R, Darra F, Bernardina BD et al. 2011. Spectrum of phenotypes in female patients with epilepsy due to protocadherin 19 mutations. *Epilepsia*. 52:1251–1257.
- Travers BG, Adluru N, Ennis C, Tromp DPM, Destiche D, Doran S, Bigler ED, Lange N, Lainhart JE, Alexander AL. 2012. Diffusion tensor imaging in autism spectrum disorder: a review. *Autism Res*. 5:289–313.
- Treble A, Juranek J, Stuebing KK, Dennis M, Fletcher JM. 2013. Functional significance of atypical cortical organization in Spina Bifida Myelomeningocele: relations of cortical thickness and gyrification with IQ and fine motor dexterity. *Cereb Cortex*. 23:2357–2369.
- Trivisano M, Pietrafusa N, Terracciano A, Marini C, Mei D, Darra F, Accorsi P, Battaglia D, Caffi L, Canevini MP et al. 2018. Defining the electroclinical phenotype and outcome of PCDH19-related epilepsy: a multicenter study. *Epilepsia*. 59:2260–2271.
- Vuoksima E, Panizzon MS, Chen C-H, Fiecas M, Eyler LT, Fennema-Notestine C, Hagler DJ, Fischl B, Franz CE, Jak A et al. 2015. The genetic association between neocortical volume and general cognitive ability is driven by global surface area rather than thickness. *Cereb Cortex*. 25:2127–2137.
- Wallace GL, Robustelli B, Dankner N, Kenworthy L, Giedd JN, Martin A. 2013. Increased gyrification, but comparable surface area in adolescents with autism spectrum disorders. *Brain*. 136:1956–1967.
- White T, Su S, Schmidt M, Kao CY, Sapiro G. 2010. The development of gyrification in childhood and adolescence. *Brain Cogn*. 72:36–45.
- Zilles K, Palomero-Gallagher N, Amunts K. 2013. Development of cortical folding during evolution and ontogeny. *Trends Neurosci*. 36:275–284.